Journal Name

Dynamic Article Links ►

Cite this: DOI: 10.1039/c0xx00000x

www.rsc.org/xxxxxx

ARTICLE TYPE

Magneto-Optical Nanomaterial: a SPIO-Phthalocyanine scaffold built *step-by-step* towards bimodal imaging

Julien Boudon,[a] Jérémy Paris,[a] Yann Bernhard,[b] Elena Popova,[c] Richard A. Decréau*[b] and Nadine Millot*[a]

DOI: 10.1039/b000000x

[a] Laboratoire Interdisciplinaire Carnot de Bourgogne (ICB), UMR 6303 CNRS-Université de Bourgogne, BP 47870, F-21078, Dijon Cedex, France. E-mail: Nadine.Millot@u-bourgogne.fr
[b] Institut de Chimie Moléculaire de l'Université de Bourgogne (ICMUB), UMR 6302 CNRS-Université de Bourgogne, BP 47870, F-21078, Dijon Cedex, France; E-mail: Richard.Decreau@u-bourgogne.fr
[c] Groupe d'étude de la matière condensée (GEMaC), UMR 8635 CNRS-Université de Versailles St-Quentin-en-Yvelines, F-78035 Versailles, France.

Outline

Preamble

For clarity purposes simple labels are used all along the manuscript text:

- Initial SPIO NPs bearing hydroxyl moieties are labelled **SPIO–OH**
- Second stage SPIO NPs, SPIO–OH reacted with APTES leading to SPIO–O–Si–$(CH_2)_3$–NH_2 are labelled **SPIO–NH_2**
- Third stage SPIO NPs, SPIO-NH_2 reacted with HOOC–PEG_9–N_3 leading to SPIO–O–Si–$(CH_2)_3$–NH–C=O–PEG_9–N_3 are labelled **SPIO–N_3**
- Fourth stage SPIO NPs, SPIO–N_3 reacted with ZnPc–C≡H leading SPIO–O–Si–$(CH_2)_3$–NH–C=O–PEG_9–triazole–ZnPc are labelled **SPIO–Pc**

1. Materials, Methods and Instrumentation

Chemicals.

Chemicals used in this study are from various providers: Acros Organics [4-bromophenol (97 %, ref. 304411000), copper iodide (99.9 %, ref. 201500050), 1,8-diazabicyclo[5.4.0]undec-7-ene (98 %, ref. 160615000), 1,2-dicyanobenzene (98 %, ref. 174012500), dimethylsulfoxide (> 99.7%, ref. 34844), octanol (99 %, ref. 150630020), tetrakis(triphenylphosphine) palladium (99 %, ref. 202380010), triethylamine (99 %, ref. 157910010), zinc acetate dihydrate (98 %, ref. 207640010)], Carlo Erba [potassium carbonate (pure, 359809)], Fisher Chemicals [nitric acid for SPIO peptisation (68%, ref. N/2300/PB17), THF (BHT-stabilized, ref. T/0701/21)], Fluka [N-(3-dimethylaminopropyl)-N□-ethylcarbodiimide hydrochloride (≥ 98%, ref. 03450)], IRIS Biotech [32-azido-5-oxo-3,9,12,15,18,21,24,27,30-nonaoxa-6-azadotriacontan-1-oic acid (554.59 $g.mol^{-1}$, ref. PEG2015)], Sigma-Aldrich [3-aminopropyltriethoxysilane (≥ 98%, ref. A3648), dimethylformamide (>99%, ref. 15440), ethynyltrimethyl-silane (98 %, ref. 101061688), $FeCl_3$•$6H_2O$ (≥ 98%, ref. F2877), $FeCl_2$•$4H_2O$ (98%, ref. 220299), N-hydroxysuccinimide (98%, ref. 130672), sodium hydroxide pellets (≥ 98%, ref. S5881) and TCI [4-nitro-1,2-dicyanobenzene (TCI, >98 %, ref. N0524)]. Chemicals were used as received without any further purification when no otherwise stated.

Characterizations.

Chromatography.

Compound **3** was purified on column chromatography using silica gel (60A, SDS) and a specific mixture of solvent as described in section 2.

DLS and Zeta Potential

Hydrodynamic diameter and zeta potential measurements were performed on a Zeta-Nanosizer (Malvern) into 10^{-2} M NaCl solutions.

ESI-Q MS

(ElectroSpray Ionisation-Quadripole Mass Spectroscopy): measurements were performed on LTQ Orbitrap XL (THERMO) coupled to HPLC Ultimate 3000 (DIONEX); 1 mg compound into 1 mL DCM.

Fluorimeter.

Fluorolog Jobin Yvon Hobiba equipped with a Xe source. Fluorescence spectra for free ZnPc and conjugate **1** were recorded in THF and ethanol, respectively. Excitation was performed at 600 nm and emission band was observed around 673 nm.

Fourier Transformed InfraRed spectroscopy (FTIR).

Measurements were performed on a FTIR Bruker Vertex 70v spectrometer; samples were analyzed on KBr pellets, which were prepared as follows: KBr powder (150 mg) and powder sample (2 mg) were mixed and pressed. SPIO NPs FTIR spectra were recorded on a BRUKER IFS 28 and processed by OPUS software: depending on their nature, samples were analyzed as powders into dried KBr or as liquids through an ATR device

ICP

Measurements were performed on a ThermoScientific cAP 6000 series ICP Spectrometer, on a SPIO–Pc powder (2 mg) mixed in 5:1 volumic ratio of HCl/H_2O_2 (3 mL, 12 and 9.8 mol/L respectively) to decompose the SPIO leading to a light yellow clear homogeneous solution. The resulting mixture was diluted with water to 10 mL, and two sets of solutions were analyzed, 1/10 and 1/50 dilutions.

Magnetic Measurements

Measurements were performed on a Physical Property Measurement System (PPMS). Magnetic properties of bare SPIO nanoparticles and functionalized SPIO–Pc were measured. The hysteresis curves were recorded at 300 K in [-1 T; 1 T] range. In order to determine the blocking temperature,

magnetic moment of each sample was measured at applied field of 10^{-2} T while heating from 5 K to 320 K after zero field cooled (at 0 T) and field cooled (at 10^{-2} T) procedure.

MALDI-TOF MS

(Matrix-Assisted Laser Desorption/Ionisation - Time of Flight Mass Spectroscopy). Measurements were performed on Ultraflex II LRF 2000 (BRUKER); matrix used: dithranol; 1 mg compound into 1 mL DMSO.

NMR spectroscopy.

Measurements were performed on a Bruker Dalton X, at 300 MHz (^{1}H), or 75 MHz (^{13}C). Phthalocyanines precursors **3**, **4** were analyzed in $CDCl_3$ and free phthalocyanines samples **2** into DMSO-d_6 (*ca*. 5-10 mg/400 µL (^{1}H-NMR), and twice as much for ^{13}C-NMR). Chemical shifts are expressed in ppm relative to TMS (deuterated chloroform chemical shift was set at 7.26 ppm).

Photobleaching experiment

Continuous Irradiation (over 900 minutes) of the samples was achieved using a Xenon lamp, at the excitation wavelength of each fluorophore (*i.e*. λ_{ex}(fluorescein) = 470 nm / λ_{em}(fluorescein) = 540 nm; λ_{ex}(phthalocyanine) = 610 nm / λ_{em}(phthalocyanine) = 674 nm) and 0.5 nm slits (emission) and 0.5 nm slit (excitation). The solution of fluorophore in DMSO (fluoresceine) or 1-chloronaphthalene (phthalocyanine) was placed in a quartz cuvette (1 cm pathlength). The absorbance was measured every 30 seconds over 900 minutes.

Relaxivity measurements.

Measurements were performed on a Bruker Minispec mqvar ND2318. Relaxation measurements were performed at 40°C (*i.e*. close to the physiological temperature), suspensions were stable enough during the experiments to be measured in water, 500 μL in an NMR tube. For each of the six suspensions examined five measurements were realized.

Surface area measurement.

Measurements were performed using a BELSORP-mini apparatus with N_2 gas adsorption. The BET method has been used in the calculation of surface area values (S_{BET}) from the isotherm of nitrogen adsorption.

TEM

Transmission Electron Microscopy images were obtained from a JEOL JEM 2100 LaB_6 operating at 200 kV (point resolution 2.5 Å). The copper grids were dipped in dilute suspension of samples in ethanol and naturally dried.

ThermoGravimetric Analysis (TGA).

Desorption of NPs and decomposition of the organic compounds were studied by thermogravimetry (SETARAM TAG24). This symmetric thermobalance is able to measure weight variations of 0.1 µg. Heating rate was 2°C up to 800°C N_2/O_2 (120/40 mL/min). Sample weight was 5-10 mg.

UV-Visible spectroscopy.

ZnPc and SPIO NPs spectra were performed on a Shimadzu UV-2550 spectrophotometer. Free phthalocyanines spectra were recorded in THF; SPIO–Pc conjugate **1** spectra were recorded either in ethanol or in DMSO into glass cuvettes 1x1x3 cm (1 cm path). . Other samples were measured as particle suspensions into ultrapure water (resistivity 18 MΩ) when no otherwise stated.

XPS.

X-ray Photoelectron Spectroscopy data were recorded on a PHI Versaprobe 5000 device and Al–Kα monochromated radiation (1486.6 eV, 50 W with a 200-μm-diameter spot size) was used as X-ray source. Pass energy is 200 eV for spectra and 60 eV for windows (quantifications and curve fitting are obtained from windows acquisitions). Powder samples were prepared by pressing the sample powder on an indium sheet. Neutralization was used to minimize charge effects and the adventitious carbon C1s peak at 284.5 eV was used as the reference. The pressure in analysis chamber during acquisition is around 8.10^{-8} Pa.

Photoemission peak areas were calculated after background subtraction using a Shirley routine and all concentration calculations were done with Multipack software. Windows were decomposed into components by fitting with Gaussian (70%)-Lorentzian (30%) peaks. In the fitting procedure, Full-Widths at Half-Maximum (FWHMs) were set with Casa XPS software.

X-Ray Diffraction.

X-ray diffraction (XRD) data were collected at room temperature for 24 hours using a Siemens D5000 automatic powder diffractometer, operating at 35 mA and 50 kV. Fluorescence effects were minimized by using Cu K_β radiation (1.39222 Å). The lattice parameters and the crystallite size ($Ø_{XRD}$) calculations were obtained using the Topas software from Bruker.

2. Syntheses and purification

Bare SPIO NPs.

A solution of 1:2 molar ratio of ferrous and ferric chloride (respectively, 1 and 2 $mol.L^{-1}$) was added dropwise to a 0.75 $mol.L^{-1}$ NaOH solution at 90°C in a 2-liter flask equipped with mechanical stirrer under vigorous stirring. The product was magnetically settled down and washed three times with 400 mL of 1 M HNO_3. The NPs were stirred with 200 mL water for 5 minutes then 200 mL of 1 M HNO_3 was added and the supernatant was once more magnetically decanted. This step was repeated four times. Finally the particle suspension was centrifuged at 450 ×g for one hour to remove the biggest aggregates and the SPIO-containing supernatant was kept. The latter NPs were dispersed into water and dialyzed against an HNO_3 solution (pH 4) in 3.5 kDa MWCO dialysis tubing for 24 hours.

SPIO–NH_2.

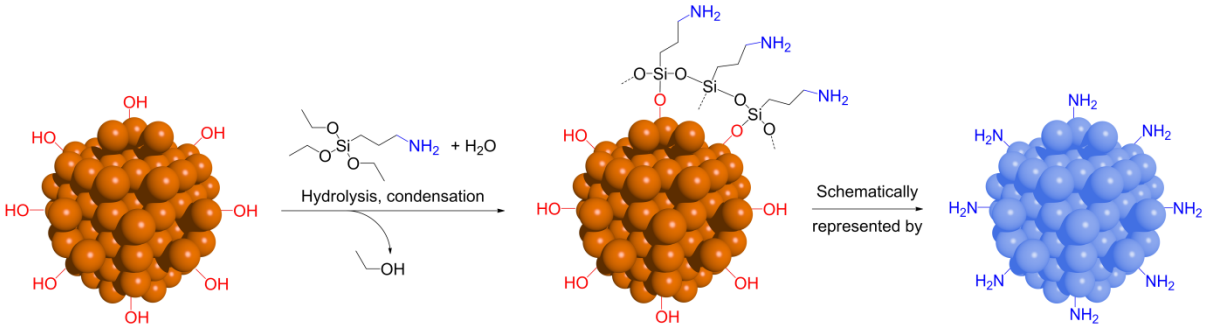

Bare SPIO NPs were subjected to 3-aminopropyltriethoxysilane (APTES) in an equivalent mass ratio into 20 mL of a 1:1 ethanol/water mixture, the pH of which is decreased to 4 by the addition of 1 M HCl prior to the APTES addition. The mixture was submitted to an ultrasonic treatment (225 W, 3 min, Sonics Vibra-Cells) to afford a good particle dispersion leading to the polysiloxane coverage of individual particles rather than agglomerates. The mixture was then submitted to mechanical stirring (60 rpm) during 48 h. 20 mL of glycerol was then added followed by the evaporation of the ethanol/water mixture under reduced pressure to increase the polysiloxane condensation around SPIO NPs. Finally, glycerol was removed by acetone addition to the SPIO NP suspension accompanied by a magnetic decantation. SPIO NPs were finally re-suspended into ultrapure water yielding SPIO–NH_2 and dialysed one week against ultrapure water (resistivity 18 MΩ).

SPIO–N_3.

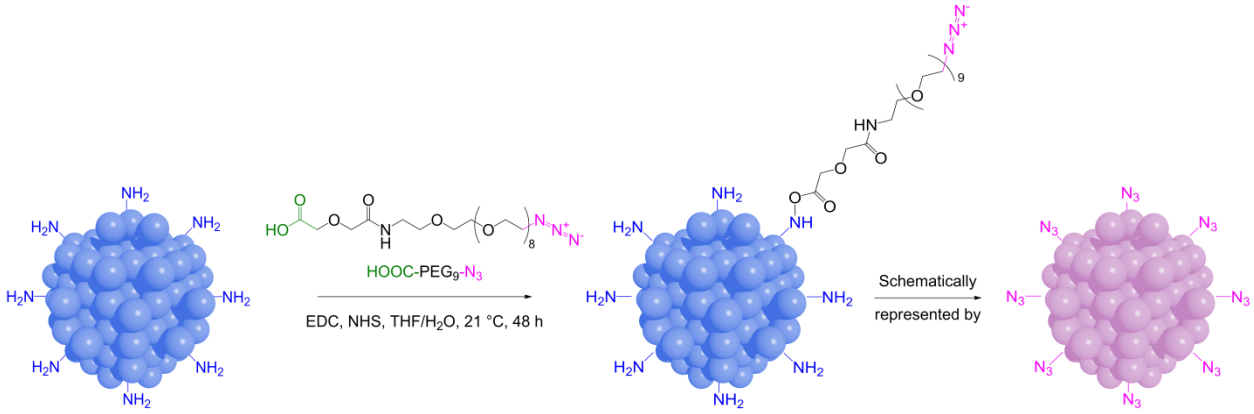

SPIO–NH_2 NPs were subjected to an equivalent mass ratio of 32-azido-5-oxo-3,9,12,15,18,21,24,27,30-nonaoxa-6-azadotriacontan-1-oic acid (N_3–PEG_9–COOH) in the presence of

N-(3-dimethylaminopropyl)-*N'*-ethylcarbodiimide hydrochloride (EDC) and *N*-hydroxysuccinimide (NHS, dissolved into DMSO) at 1.0 and 1.1 molar equivalent respectively with respect to the PEG stoichiometry. The mixture was stirred (60 rpm) in 15 mL of 1:1 THF/water at pH 5.1 during 48 h followed by magnetic decantation into THF and ultrafiltration against ethanol leading to SPIO–N_3 NPs. Because azide derivatives decompose explosively upon heating, no TGA was realized at this stage.

4-(4-bromophenoxy)phthalonitrile (4).

A mixture of 4-nitro-phthalonitrile (1 g, 5.8 mmol), 3-bromophenol (1 g, 5.8 mmol) and potassium carbonate (1.6 g, 11.6 mmol) was stirred in DMF (20 mL) at room temperature during 2 hours. After addition of 20 mL of water, the resulting precipitate was filtered off and washed with water (3×10 mL). The white-pink solid obtain was dry under reduce pressure to afford compound 4 (1.73 g, 95%).

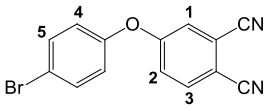

^{1}H NMR (300 MHz, DMSO-d_6, 298 K): δ (ppm)= 7.31 (d, ^{3}J= 8.8 Hz, 2H, H_5); 7.58 (dd, ^{3}J= 8.6 Hz, ^{4}J= 2.6 Hz, 1H, H_2); 7,63 (d, ^{4}J= 2.6 Hz, 1H, H_1); 7.92 (d, ^{3}J= 8.8 Hz, 2H, H_4); 8,08 (d, ^{3}J= 8.6 Hz, 1H, H_3).

4-(4-((trimethylsilyl)ethynyl)phenoxy)phthalonitrile (3).

A solution of trimethylsilylacetylene (328 mg, 3.34 mmol) in triethylamine (20 mL) was added to a mixture of de 4-(4-bromophenoxy)phthalonitrile **(4)** (0.5 g, 1.67 mmol), palladium (tetrakis-triphenyl)phosphine (193 mg, 0.167 mmol) and copper iodide (159 mg, 0.835 mmol) under argon atmosphere. The mixture was heated at 60 °C during 2 hours. After addition of DCM (30 mL), the organic layer was washed with brine (3×30 mL), saturated NH_4Cl solution (3×30 mL), water (30 mL) and dried with $MgSO_4$. The solvent was evaporated and the resulting oil was purified by column

chromatography (hexane/AcOEt, 80:20) to obtain 4-(4-((trimethylsilyl)ethynyl)phenoxy)phthalonitrile **(3)** as a white powder (400 mg, 77 %).

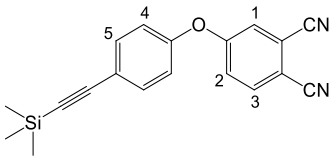

^{1}H NMR (300 MHz, $CDCl_3$, 298 K): δ (ppm) = 0.11 (s, 9H, $Si(CH_3)_3$); 6.85 (d, ^{3}J= 8.7 Hz, 2H, H_5); 7.07 (dd, ^{3}J= 8.5 Hz, ^{4}J= 2.6 Hz, 1H, H_2); 7.13 (d, ^{4}J= 2.6 Hz, 1H, H_1); 7.39 (d, ^{3}J= 8.6 Hz, 2H, H_4); 7.57 (d, ^{3}J= 8.7 Hz, 1H, H_3). ^{13}C NMR (75 MHz, $CDCl_3$, 298 K): δ (ppm) = 5.1; 100.0; 110.0; 114.1; 120.6; 121.1; 122.1; 125.5; 124.7; 128; 128.5; 139.2; 141.6; 159.6; 165.4. ESI-Q MS m/z calc.: 339.3 $[M+Na]^+$. Anal. Calc. For $C_{19}H_{16}N_2OSi$: C, 71.18 %, H, 5.10 %, N, 8.42 %.

2-(4-(alkynyl)phenoxy)-phthalocyaninato zinc(II) (2).

A suspension of 4-(4-((trimethylsilyl)ethynyl)phenoxy)phthalonitrile (3) (0.4 g, 1.26 mmol), phthalonitrile (1.13 g, 8.82 mmol), zinc acetate dihydrate (553 mg, 2.52 mmol), in octanol (10 mL) and 1,8-diazabicyclo[5.4.0]undec-7-ene (1.5 mL, 10.1 mmol) was heated at 130 °C during 2 hours. Then the reaction mixture was cooled to 21 °C and the blue precipitate was filtered off, washed with 1 M hydrochloric acid (3×20 mL), water (3×20 mL) and methanol (10 mL), then subsequently washed with dichloromethane for 12 h in a Soxhlet extractor. The blue solid was dried under reduced pressure to afford the mixture of non-substituted A_4-ZnPc and mono-substituted A_3B-ZnPc phthalocyanine (where A_4 stands for four unsubstituted isoindoles of the ZnPc and A_3 for three unsubstituted isoindoles, B stands for the alkyne-containing isoindole; 400 mg of mixture, 23 % estimated yield for the mono-substituted A_3B-ZnPc, calculated by integration on the ^{1}H NMR spectrum).

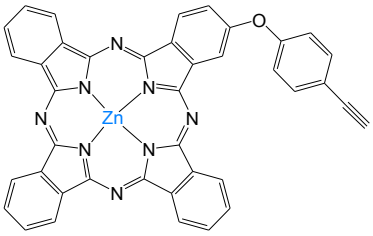

^{1}H NMR (300 MHz, DMSO-d_6, 298 K): δ (ppm) = 4.28 (s, 1H, $H_{alkynyl}$); 7.55 (d, J= 8.0 Hz, 2H, $H_{phenoxy}$); 7.67 (d, J= 8.1 Hz, 1H) 7.81 (d, J= 8. 0 Hz, 2H, $H_{phenoxy}$), 8.1 (m, 17H); 8.3 (s, 1H); 8.77 (d, J= 6.4 Hz, 1H); 8.90 (m, 2H); 8.99 (m, 14 H). MALDI-TOF MS m/z calc. 576.23 $[M+H]^+$ (ZnPc); 576.23 $[M+H]^+$ (z). UV-Vis (DMSO), λ_{max} (nm) (.10^3 ε): 344.1 (41.3), 602.9 (21.3), 640.0 (19.5), 667.4 (142.2).

SPIO–Pc

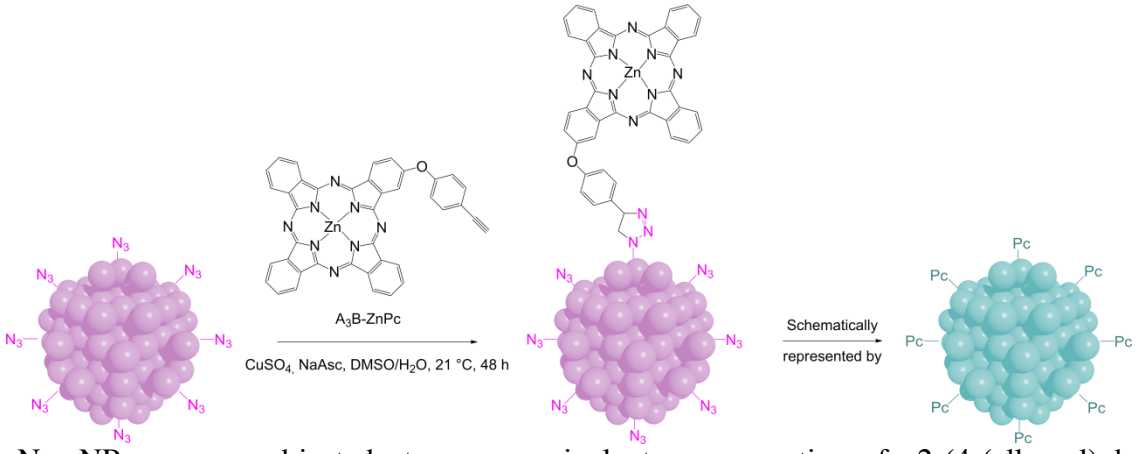

SPIO–N_3 NPs were subjected to an equivalent mass ratio of 2-(4-(alkynyl)phenoxy)-phthalocyaninato zinc(II) (alkyne-containing A_3B-ZnPc **2**) in the presence of $CuSO_4$ (5.5 molar equivalent) and sodium ascorbate (3.5 molar equivalent) with respect to the alkyne-ZnPc **2** stoichiometry. The suspension was dispersed under ultrasonic treatment (225 W, 15 min, Sonics Vibra-Cells). The mixture was stirred (60 rpm) in 4:1 DMSO/water during 48 h followed by magnetic decantation into THF and ultrafiltration against ethanol leading to SPIO–Pc conjugate **1**.

3. Characterizations of the SPIO–Pc conjugate 1.

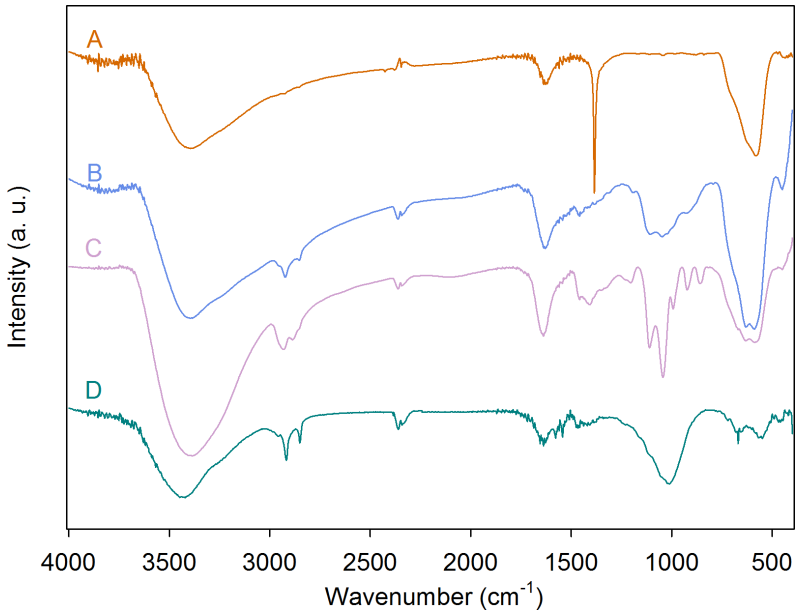

FTIR spectra of (A) SuperParamagnetic Iron Oxide (SPIO), (B) amine-grafted SPIO (SPIO–NH_2), (C) azide-grafted SPIO (SPIO–N_3) and (D) phthalocyanine-grafted SPIO (SPIO–Pc).

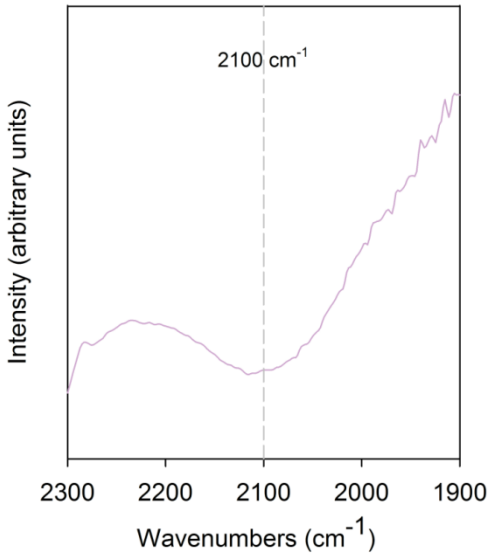

Magnification of the FTIR spectrum of azide-grafted SPIO (SPIO–N_3) in the 2300-1900 cm^{-1} region exhibiting the N_3 characteristic vibration band at 2100 cm^{-1}.

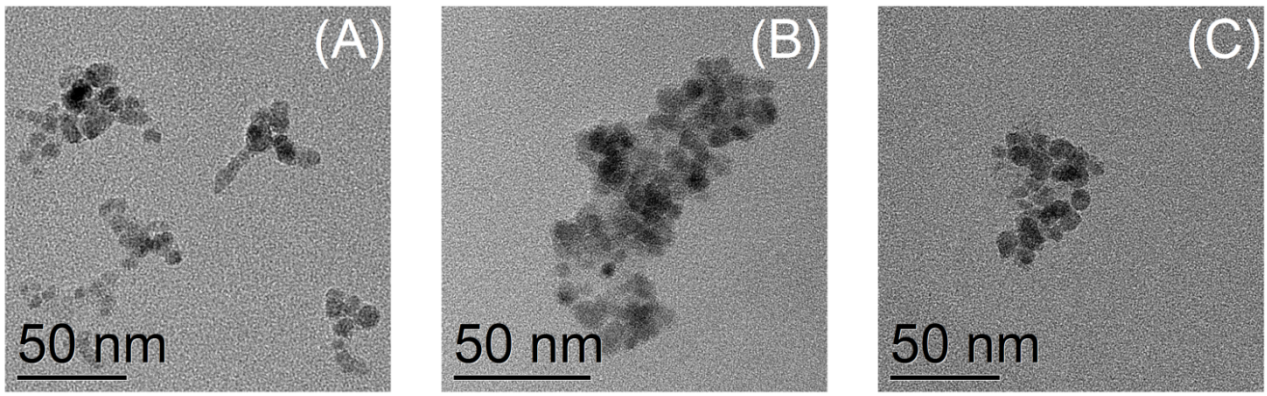

TEM micrographs showing (A) SPIO–NH_2, (B) SPIO–N_3 and (C) SPIO–Pc

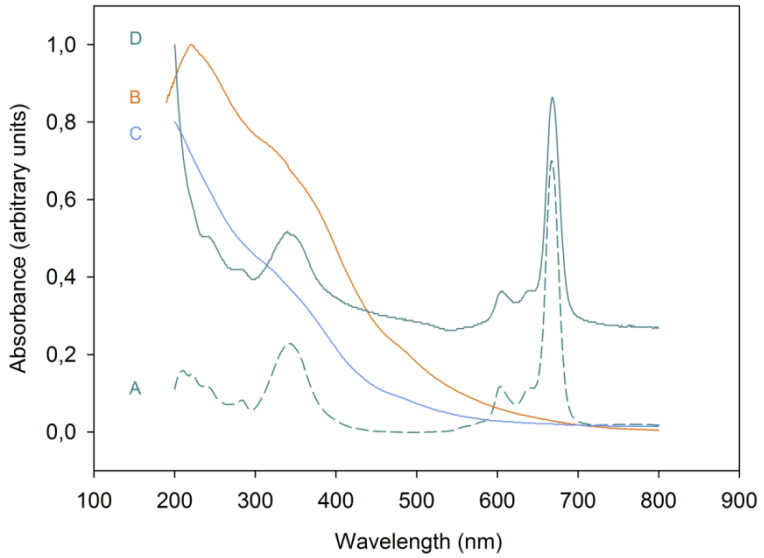

SPIO UV-Visible spectra showing (A) zinc phthalocyanine (ZnPc, dashed line), (B) SuperParamagnetic Iron Oxide (SPIO) NPs, (C) amine-grafted SPIO (SPIO–NH_2) and (D) phthalocyanine-grafted SPIO (SPIO–Pc, spectrum shifted up for clarity purposes).

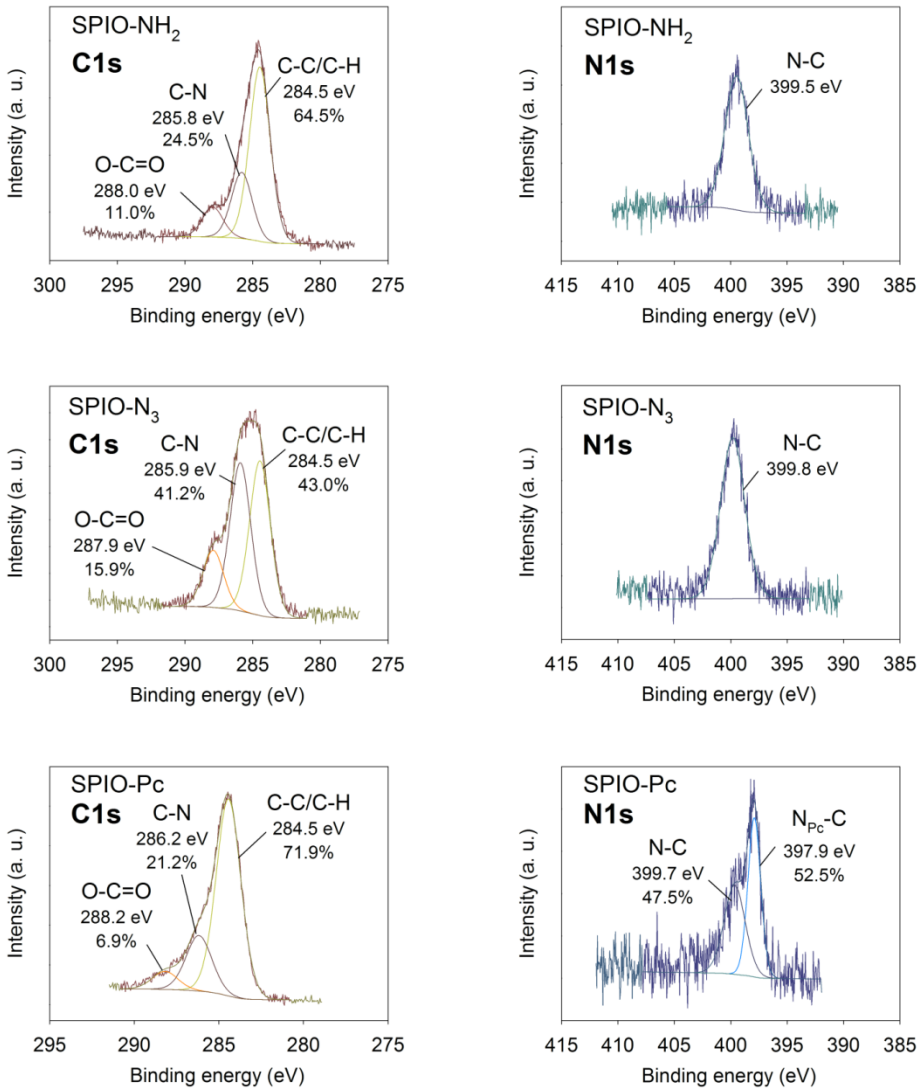

XPS spectra for C1s and N1s in amine-grafted SPIO (SPIO–NH_2), azide-grafted SPIO (SPIO–N_3) and phthalocyanine-grafted SPIO (SPIO–Pc).

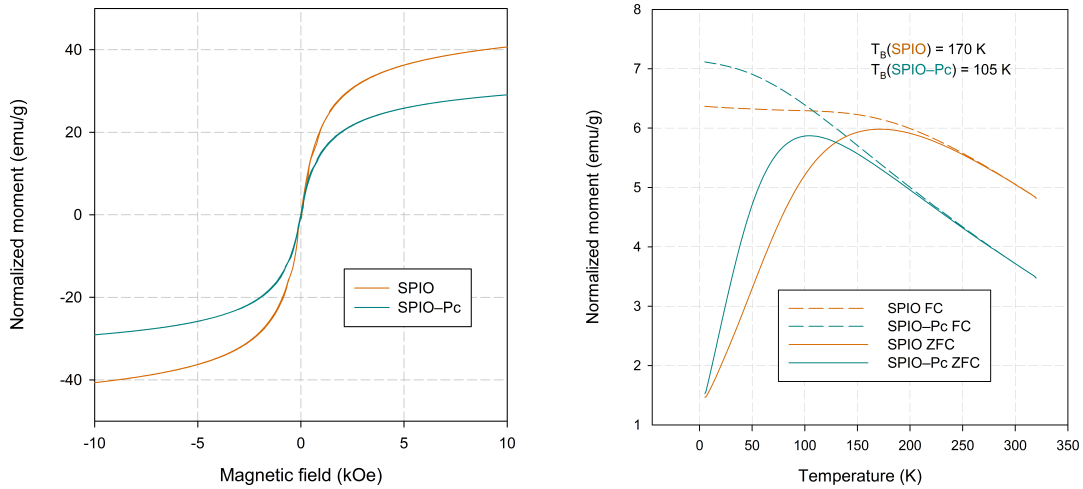

Magnetic measurements: hysteresis curves for SPIO and SPIO–Pc at 300 K (left); SPIO and SPIO–Pc field cooled (FC) and zero field cooled (ZFC) measurements between 5 K and 320 K (right).

4. Imaging Properties of the SPIO–Pc Conjugate 1

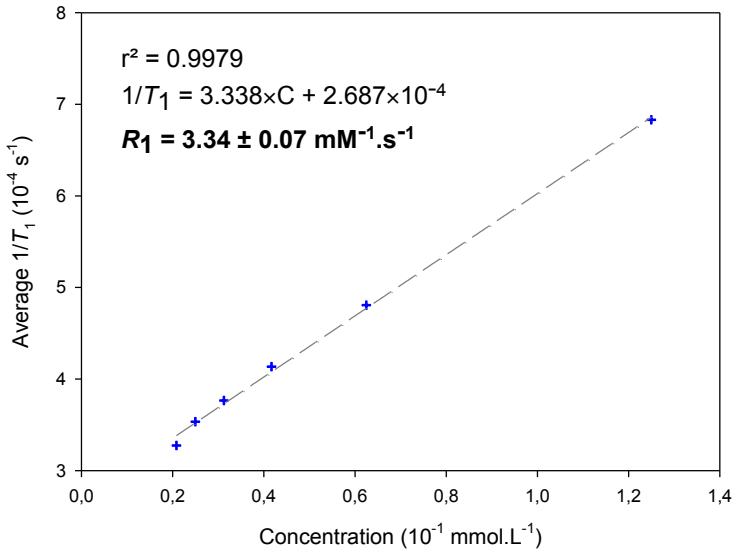

T_1 measurements vs. concentration lead to the determination of the R_1 parameter which is about 3 $mM_{Fe}^{-1}.s^{-1}$.

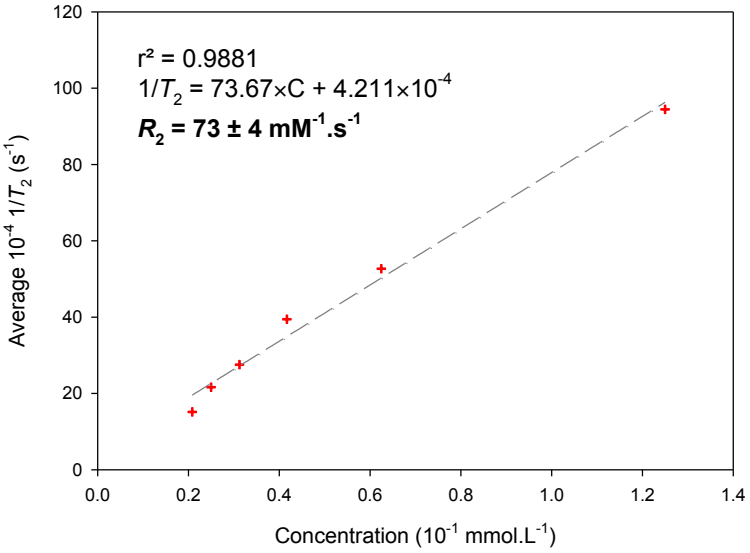

T_2 measurements vs. concentration lead to the determination of the R_2 parameter, which is about 73 $mM_{Fe}^{-1}.s^{-1}$.

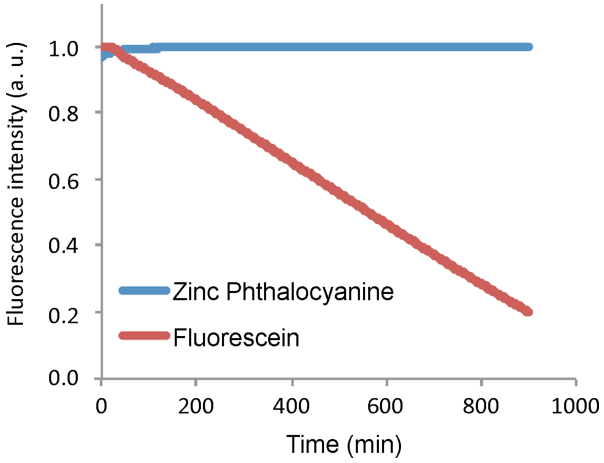

Photostability measurements: compared results over a 900 min period between fluorescein (standard fluorophore presenting fluorescence decay) and the zinc phthalocyanine used (photostable fluorophore).

5. Calculation of Zinc phthalocyanine coverage on SPIO NPs

Provided that the SPIO NPs morphology is between spherical and cubic, the least favorable case is used to calculate the minimum coverage of phthalocyanine, *i.e.* the sphere surface area is considered (indeed the surface of a cube is almost twice higher the one of a sphere; $6\times(2R)^2 / (4\pi R^2) = 6/\pi \approx 1.9$).

The coverage is calculated as follows:

$$\mathcal{C} = \frac{C_{Zn}\times 3M(Fe)\times \mathcal{N}\times \mathcal{A}}{C_{Fe}\times M(Fe_3O_4)\times SSA\times M(Zn)} = \frac{0.5\times 167.535\times 6.022\ 10^{23}\times 254.47\ 10^{-18}}{12\times 231.53\times 103\times 65.409} \approx 690\ \text{ZnPc/NP}$$

Where $\mathcal{C}$ is the coverage of ZnPc per nanoparticle;
C_{Zn} is the concentration of Zn determined by ICP-AES (mg/L);
M(Fe) is the molar mass of iron (g/mol);
$\mathcal{N}$ is the Avogadro constant (/mol);
$\mathcal{A}$ is the area of one spherical nanoparticle (m²) which diameter is d_{TEM} = 9 nm;
C_{Fe} is the concentration of Fe determined by ICP-AES (mg/L);
$M(Fe_3O_4)$ is the molecular weight of magnetite (g/mol);
SSA is the specific surface area of magnetite determined by the BET technique (m²/g);
M(Zn) is the molar mass of zinc.

A step-by-step demonstration is provided below:

Determination of the Nanoparticle Surface Area

ICP data: iron concentration [Fe] = 12 $mg.L^{-1}$ (1 L → 12 mg of Iron available). ICP titration carried out on the Fe_3O_4 suspension; hence the weight of Fe_3O_4 has to be calculated.

1 mole of Fe_3O_4 represents to 231.53 g (3 × 55.845 + 4 × 15.9994) and corresponds to 3 moles of iron, equivalent to 3 × 55.845 = 167.535 g of Fe. Hence, the weight of Fe_3O_4 titrated = $\frac{12\times 231.53}{167.535}$ = 16.58 mg.

We previously determined by BET that the SPIO NP's Specific Surface Area is 103 $m^2.g^{-1}$.

Hence, the surface area of the NPs available becomes: $\frac{103 \times 16.58\ 10^{-3}}{1}$ = 1.708 m^2 of Fe_3O_4.
(or 1.708 10^{18} nm^2 Fe_3O_4). This allows us to proceed to the next step, *i.e.* the number of Pc per nm^2.

Number of Pc
ICP data: zinc concentration [Zn] = 0.5 mg $.L^{-1}$ (1 L → 0.5 mg zinc)
Pc molecular weight: M(ZnPc) = 694.03 $g.mol^{-1}$; M(Zn) = 65.409 $g.mol^{-1}$
The weight of titrated Zn is $\frac{0.5 \times 694.03}{65.409}$ = 5.31 mg Pc.
Hence, it gives the mole number of Pc: n(ZnPc) = 7.64 × 10^{-6} mol, which corresponds to 4.60 10^{18} ZnPc.

Surface Area of a 9 nm wide Nanoparticle
A Np is to be considered as a) either a sphere, the surface area of which is $A = 4\pi R^2 = 4 \times \pi \times (4.5)^2$ = 254.47 nm^2; b) or a cube the surface area of which is: $A = 6a^2 = 6 \times (9)^2$ = 486 nm^2.
As a result, if we average the two values it gives an average surface area of 370 nm^2.
We determined previously that in 1 L, there is 12 mg of Iron (from ICP titration), which corresponds to 4.32 10^{15} Np.

Determination of the Number of Pc per Nanoparticle
We estimated 4.60 10^{18} Pc per 1.708 10^{18} nm^2 which corresponds to 2.69 ZnPc/nm^2.
→ If we consider Nps as **spheres**, the estimate of the coverage becomes **686 ZnPc/Np** (*ca.* 690).
[→ If we considered them as cubic NPs, the coverage would be 1310 Pc/Np; and if we averaged the values obtained in the spherical and cubic cells, it would have given 998 Pc/Np)].

6. Additional bibliographic references

Additional bibliographic references are provided to have further reading on the subject covered by this communication. References are grouped in categories of interest.

A. Nanoparticles synthesis and characterization[1-6]

B. Optical imaging and phthalocyanines[7-16]

C. Magnetic resonance from SPIO[17-23]

D. Dual or multi-imaging[11, 24-30]

E. Nanoparticles for theranostic applications[16, 30-36]

1. A.-L. Papa, N. Millot, L. Saviot, R. Chassagnon and O. Heintz, Effect of Reaction Parameters on Composition and Morphology of Titanate Nanomaterials, *J. Phys. Chem. C*, 2009, **113**, 12682-12689. http://dx.doi.org/10.1021/jp903195h
2. R. Massart, Preparation of aqueous magnetic liquids in alkaline and acidic media, *IEEE Trans. Magn.*, 1981, **17**, 1247-1248. http://dx.doi.org/10.1109/TMAG.1981.1061188
3. F. Basile, C. Djega-Mariadassou, A. Banisadr and P. Poix, Preparation and crystallographic properties of the phases of the iron cobaltate ((1 - x)Fe_2CoO_4) - cobalt stannate (xCo_2SnO_4) system, *Ann. Chim. (Paris)*, 1975, **10**, 301-305.

4. P. Poix, *Liaisons interatomiques et propriétés physiques des composés minéraux*, Centre de documentation universitaire, Paris, 1968.
5. F. Bernard, J. Lorimier, V. Nivoix, N. Millot, P. Perriat, B. Gillot, J. F. Berar and J. C. Niepce, Cation Distribution in a Titanium Ferrite $Fe_{2.75}Ti_{0.25}O_4$ Measured by *in situ* Anomalous Powder Diffraction Using Rietveld Refinement, *J. Solid State Chem.*, 1998, **141**, 105-113. http://dx.doi.org/10.1006/jssc.1998.7924
6. L. Maurizi, F. Bouyer, J. Paris, F. Demoisson, L. Saviot and N. Millot, One step continuous hydrothermal synthesis of very fine stabilized superparamagnetic nanoparticles of magnetite, *Chem. Commun.*, 2011, **47**. http://dx.doi.org/10.1039/C1CC15470B
7. A. F. Fercher, W. Drexler, C. K. Hitzenberger and T. Lasser, Optical coherence tomography - principles and applications, *Rep. Prog. Phys.*, 2003, **66**, 239. http://dx.doi.org/10.1088/0034-4885/66/2/204
8. E. Ben-Hur and W.-S. Chan, in *Porphyrin Handbook*, eds. K. M. Kadish, K. M. Smith and R. Guilard, Elsevier Science, USA, 2003, vol. 19, pp. 1-35.
9. R. A. Decréau, M. Chanon and M. Julliard, Synthesis of Silicon Phthalocyanines Bearing Two Cholesterol Moieties, *Synlett*, 1998, 375-376. http://dx.doi.org/10.1055/s-1998-1661
10. N. Nombona, E. Antunes, C. Litwinski and T. Nyokong, Synthesis and photophysical studies of phthalocyanine-gold nanoparticle conjugates, *Dalton Transactions*, 2011, **40**, 11876-11884. http://dx.doi.org/10.1039/C1DT11151E
11. H.-J. Kim, K.-J. Shin, M. K. Han, K. An, J.-K. Lee, I. Honma and H. Kim, One-pot synthesis of multifunctional mesoporous silica nanoparticle incorporated with zinc(II) phthalocyanine and iron oxide, *Scripta Mater.*, 2009, **61**, 1137-1140. http://dx.doi.org/10.1016/j.scriptamat.2009.09.001
12. W. Alves, A. O. Ribeiro, M. V. B. Pinheiro, K. Krambrock, F. E. Haber, G. Froyer, O. Chauvet, R. A. Ando, F. L. Souza and W. A. Alves, Quenching of Photoactivity in Phthalocyanine Copper(II) - Titanate Nanotube Hybrid Systems, *J. Phys. Chem. C*, 2011, **115**, 12082-12089. http://dx.doi.org/10.1021/jp202101r
13. C. Wanxi, S. Yue, W. Guizhi, G. Feng, Z. Jiancheng and W. Linjun, Preparation and properties of a phthalocyanine-sensitized TiO 2 nanotube array for dye-sensitized solar cells, *Semiconductor Science and Technology*, 2010, **25**, 125014. http://dx.doi.org/10.1088/0268-1242/25/12/125014
14. R. A. Decréau, J. P. Collman, Y. Yang, Y. Yan and N. K. Devaraj, Syntheses of Hemoprotein Models that can be Covalently Attached onto Electrode Surfaces by Click Chemistry, *J. Org. Chem.*, 2007, **72**, 2794-2802. http://dx.doi.org/10.1021/jo062349w
15. R. A. Decréau, M. J. Richard, P. Verrando, M. Chanon and M. Julliard, Photodynamic activities of silicon phthalocyanines against achromic M6 melanoma cells and healthy human melanocytes and keratinocytes, *J. Photochem. Photobiol. B: Biol.*, 1999, **48**, 48-56. http://dx.doi.org/10.1016/S1011-1344(99)00008-1
16. M. Camerin, M. Magaraggia, M. Soncin, G. Jori, M. Moreno, I. Chambrier, M. J. Cook and D. A. Russell, The in vivo efficacy of phthalocyanine–nanoparticle conjugates for the photodynamic therapy of amelanotic melanoma, *Eur. J. Cancer*, 2010, **46**, 1910-1918. http://dx.doi.org/10.1016/j.ejca.2010.02.037
17. M. Hofmann-Amtenbrink, H. Hofmann and X. Montet, Superparamagnetic nanoparticles - a tool for early diagnostics, *Swiss Med. Wkly.*, 2010, **140**, 7-13. http://dx.doi.org/10.4414/smw.2010.13081
18. A. M. Hamilton, K. A. Rogers, A. J. L. Belisle, J. A. Ronald, B. K. Rutt, R. Weissleder and D. R. Boughner, Early identification of aortic valve sclerosis using iron oxide enhanced MRI, *J. Magn. Reson. Imaging*, 2010, **31**, 110-116. http://dx.doi.org/10.1002/jmri.22008
19. E. Pöselt, H. Kloust, U. Tromsdorf, M. Janschel, C. Hahn, C. Maßlo and H. Weller, Relaxivity Optimization of a PEGylated Iron-Oxide-Based Negative Magnetic Resonance Contrast Agent for T2-Weighted Spin–Echo Imaging, *ACS Nano*, 2012, **6**, 1619-1624. http://dx.doi.org/10.1021/nn204591r
20. E. D. Smolensky, H.-Y. E. Park, T. S. Berquó and V. C. Pierre, Surface functionalization of magnetic iron oxide nanoparticles for MRI applications – effect of anchoring group and ligand exchange protocol, *Contrast Media Mol. Imaging*, 2011, **6**, 189-199. http://dx.doi.org/10.1002/cmmi.417

21. K. Morishige, D. F. Kacher, P. Libby, L. Josephson, P. Ganz, R. Weissleder and M. Aikawa, High-Resolution Magnetic Resonance Imaging Enhanced With Superparamagnetic Nanoparticles Measures Macrophage Burden in Atherosclerosis, *Circulation*, 2010, **122**, 1707-1715. http://dx.doi.org/10.1161/circulationaha.109.891804
22. M. Amanlou, S. D. Siadat, D. Norouzian, S. E. S. Ebrahimi, M. R. Aghasadeghi, M. Ghorbani, M. S. Alavidjeh, D. N. Inanlou, A. J. Arabzadeh and M. S. Ardestani, Magnetic resonance contrast media sensing in vivo molecular imaging agents: an overview, *Curr. Radiopharm.*, 2011, **4**, 31-43. http://dx.doi.org/10.2174/1874471011104010031
23. D. E. Sosnovik, E. A. Schellenberger, M. Nahrendorf, M. S. Novikov, T. Matsui, G. Dai, F. Reynolds, L. Grazette, A. Rosenzweig, R. Weissleder and L. Josephson, Magnetic resonance imaging of cardiomyocyte apoptosis with a novel magneto-optical nanoparticle, *Magn. Reson. Med.*, 2005, **54**, 718-724. http://dx.doi.org/10.1002/mrm.20617
24. S. L. Pimlott and A. Sutherland, Molecular tracers for the PET and SPECT imaging of disease, *Chem. Soc. Rev.*, 2011, **40**, 149-162. http://dx.doi.org/10.1039/B922628C
25. T. J. Wadas, E. H. Wong, G. R. Weisman and C. J. Anderson, Coordinating Radiometals of Copper, Gallium, Indium, Yttrium, and Zirconium for PET and SPECT Imaging of Disease, *Chem. Rev.*, 2010, **110**, 2858-2902. http://dx.doi.org/10.1021/cr900325h
26. P. S. Mackay, G.-J. Kremers, S. Kobukai, J. G. Cobb, A. Kuley, S. J. Rosenthal, D. S. Koktysh, J. C. Gore and W. Pham, Multimodal imaging of dendritic cells using a novel hybrid magneto-optical nanoprobe, *Nanomed. Nanotechnol. Biol. Med.*, 2011, **7**, 489-496. http://dx.doi.org/10.1016/j.nano.2010.12.004
27. R. Torres Martin de Rosales, R. Tavaré, A. Glaria, G. Varma, A. Protti and P. J. Blower, ^{99m}Tc-Bisphosphonate-Iron Oxide Nanoparticle Conjugates for Dual-Modality Biomedical Imaging, *Bioconjugate Chem.*, 2011, **22**, 455-465. http://dx.doi.org/10.1021/bc100483k
28. Z. Ali, A. Z. Abbasi, F. Zhang, P. Arosio, A. Lascialfari, M. F. Casula, A. Wenk, W. Kreyling, R. Plapper, M. Seidel, R. Niessner, J. Knöll, A. Seubert and W. J. Parak, Multifunctional Nanoparticles for Dual Imaging, *Anal. Chem.*, 2011, **83**, 2877-2882. http://dx.doi.org/10.1021/ac103261y
29. A.-L. Puaux, L. C. Ong, Y. Jin, I. Teh, M. Hong, P. K. H. Chow, X. Golay and J.-P. Abastado, A Comparison of Imaging Techniques to Monitor Tumor Growth and Cancer Progression in Living Animals, *Int. J. Mol. Imag.*, 2011, **2011**. http://dx.doi.org/10.1155/2011/321538
30. X.-X. Meng, J.-Q. Wan, M. Jing, S.-G. Zhao, W. Cai and E.-Z. Liu, Specific targeting of gliomas with multifunctional superparamagnetic iron oxide nanoparticle optical and magnetic resonance imaging contrast agents1, *Acta Pharm. Sin.*, 2007, **28**, 2019-2026. http://dx.doi.org/10.1111/j.1745-7254.2007.00661.x
31. C. Tassa, S. Y. Shaw and R. Weissleder, Dextran-Coated Iron Oxide Nanoparticles: A Versatile Platform for Targeted Molecular Imaging, Molecular Diagnostics, and Therapy, *Acc. Chem. Res.*, 2011, **44**, 842-852. http://dx.doi.org/10.1021/ar200084x
32. P. Wust, B. Hildebrandt, G. Sreenivasa, B. Rau, J. Gellermann, H. Riess, R. Felix and P. M. Schlag, Hyperthermia in combined treatment of cancer, *The Lancet Oncology*, 2002, **3**, 487-497. http://dx.doi.org/10.1016/s1470-2045(02)00818-5
33. T.-G. Iversen, T. Skotland and K. Sandvig, Endocytosis and intracellular transport of nanoparticles: Present knowledge and need for future studies, *Nano Today*, 2011, **6**, 176-185. http://dx.doi.org/10.1016/j.nantod.2011.02.003
34. M. F. Kircher, U. Mahmood, R. S. King, R. Weissleder and L. Josephson, A Multimodal Nanoparticle for Preoperative Magnetic Resonance Imaging and Intraoperative Optical Brain Tumor Delineation, *Cancer Res.*, 2003, **63**, 8122-8125.
35. J. Xie, G. Liu, H. S. Eden, H. Ai and X. Chen, Surface-Engineered Magnetic Nanoparticle Platforms for Cancer Imaging and Therapy, *Acc. Chem. Res.*, 2011, **44**, 883-892. http://dx.doi.org/10.1021/ar200044b
36. J. Xie, S. Lee and X. Chen, Nanoparticle-based theranostic agents, *Adv. Drug Del. Rev.*, 2010, **62**, 1064-1079. http://dx.doi.org/10.1016/j.addr.2010.07.009